High-Inertia Asynchronous Condenser: A New Tool Cosupporting the Voltage and Frequency of Renewable Energy Stations

Xianfei Xie, Patrick J. Palanas, Yahong Chen, Xiaozhe Li, Tianqi Xie, and Jiabing Hu, *Senior Member, IEEE*

***Abstract*—Modern power grid suffers from low short-circuit ratio and absence of mechanical inertia. Conventional synchronous condensers (SynCons) could not provide sufficient inertia (typically $H < 5$ s), and has a slow reactive power regulation speed (typically > 2 s). To address these issues, this article proposes a high-inertia asynchronous condenser (HIAC) system, which combines the advantages of SynCons, doubly-fed machines (DFMs), and flywheel energy storage. Adopting ac excitation enables HIAC to achieve wide-range speed regulation (up to $\pm$ 30%) far exceeding that of traditional synchronous machines ($\pm$ 2%), which results in the provision of high equivalent inertia. Furthermore, the high dc bus voltage of ac excitation significantly enhances power response speed. This article introduces the operational principles and characteristics of the HIAC, as well as its hierarchical control strategy and active frequency/voltage support strategy. Finally, the effectiveness of the HIAC in supporting the voltage and frequency of renewable energy stations is verified by simulations and experiments. Results proved that the HIAC could prove equivalent inertia that is more than 10 times greater than that of the conventional SynCon and achieved rapid power response of around 20 ms.**

***Index Terms*—Asynchronous condenser, frequency support control, high-inertia doubly-fed machine (DFM), voltage support control.**

NOMENCLATURE

D	Damper constant.
E_k	Rotor kinetic energy.
f_0	Nominal grid frequency.
f_g	Grid frequency.
f_{set}	Frequency set-point.
Δf_{max}	Maximum frequency deviation.
H	Inertia time constant.
I_s	Stator current.
I_r	Rotor current.
J	Rotor inertia.
K_d	Virtual inertia gain.
L_m	Mutual inductance.
L_s	Stator inductance.
L_{sl}	Stator leakage inductance.
L_{rl}	Rotor leakage inductance.
n	Rotor speed.
n_{upper}	Upper rotor speed limit.
n_{lower}	Lower rotor speed limit.
n_{max}	Maximum rotor speed.
n_{min}	Minimum rotor speed.
N	Stator/rotor turns ratio.
Ω_r	Rotor angular speed.
ω_n	Filter natural frequency.
P_c	Charging active power.
P_{dc}	Discharging active power.
P_s	Stator active power.
P_r	Rotor active power.
P_t	Total active power.
P_{max}	Maximum active power.
P_{set}	Active power set-point.
Q_s	Stator reactive power.
Q_r	Rotor reactive power.
Q_t	Total reactive power.
R_s	Stator resistance.
R_r	Rotor resistance.
$\mathcal{S}$	Laplace transform variable.
s	Slip rate.
S_n	Nominal apparent power.
T_m	Mechanical torque.
T_e	Electromagnetic torque.
U_s	Stator voltage.
X_s	Stator impedance.
ξ	Filter damping factor.

Received 3 April 2025; revised 13 July 2025 and 17 September 2025; accepted 7 November 2025. Date of publication 11 November 2025; date of current version 19 January 2026. This work was supported in part by the National Key R&D Program of China (Key Technology and Equipment for High Inertia Energy Storage Synchronous Condenser) under Grant 2023YFB2406800 and in part by the National Natural Science Foundation of China under Grant 52307054. Recommended for publication by Associate Editor B. Johnson. *(Corresponding author: Yahong Chen.)*

Xianfei Xie, Patrick J. Palanas, Xiaozhe Li, Tianqi Xie, and Jiabing Hu are with the School of Electrical and Electronic Engineering, Huazhong University of Science and Technology, Wuhan 430074, China (e-mail: xiexianfei@hust.edu.cn).

Yahong Chen is with the School of Automation, Wuhan University of Technology, Wuhan 430070, China (e-mail: yahongchen@whut.edu.cn).

Color versions of one or more figures in this article are available at https://doi.org/10.1109/TPEL.2025.3631613.

Digital Object Identifier 10.1109/TPEL.2025.3631613

I. INTRODUCTION

THE growing dominance of renewable energy in power grids has greatly reduced the short-circuit ratio and the rotational inertia, leading to voltage and frequency instability issues. Most of the currently operational inverter-based generators in the grid still lack grid support capabilities. Moreover,

additional power support relies on reserved capacity, which may become unavailable due to adverse weather conditions or other unforeseen factors. Synchronous condensers (SynCons), which could provide both voltage and inertia support to the grid, has regained attention from academia [1], [2], [3], [4]. By adjusting excitation currents, 5–6 times of the rated reactive power capacity can be delivered by the SynCon during short-circuit faults. Also, the rate of change of frequency (RoCoF) of the grid could be reduced by releasing their rotor kinetic energy during frequency events [5], [6]. Nevertheless, SynCons still suffer from certain limitations, including the following:

1) inadequate inertia, because of their limited rotor inertia and speed variation range (approximately only $\pm 2\%$ of its rated speed);
2) slower response in reactive power regulation, as the dc excitation voltage is limited (usually capped at around 5–10 p.u.).

To provide larger equivalent inertia, SynCons with additional coaxial flywheels represents an enhanced solution [7], [8]. At present, SynCons with flywheels have already been commissioned in the U.K., Italy, Australia, etc. For instance, GE supplied 8 high inertia SynCons (featuring an inertia time constant H up to 11.5 s) to Terna S.p.A. in Italy [9]. However, this type of SynCon still exhibit strong coupling between rotor speed and grid frequency, limiting their inertia support capability during frequency events due to minimal rotor speed variation range. Furthermore, the challenge of sluggish reactive power regulation speed remain unresolved.

To address the aforementioned two challenges, this article proposes a high-inertia asynchronous condenser (HIAC). The HIAC utilizes a high inertia coaxial flywheel to store kinetic energy and employs ac excitation for wide-range speed regulation, significantly enhancing equivalent inertia while also enabling rapid power regulation. The HIAC is a hybrid system that incorporates the advantages of SynCons, doubly-fed machines (DFMs) [10], and flywheel energy storage systems (FESS), such as high output power capacity (around 3 times of the inverter's capacity), wide speed regulation range (greater than $\pm$ 30%) [11], rapid regulation of active and reactive power ($<$ 20 ms), and the ability to repeatedly cycle charge and discharge. Compared to distributed static synchronous compensators (STATCOMs), it combines high equivalent inertia support capability; compared to conventional SynCons, it retains strong voltage support capability while features faster power regulation speed. Other energy storage systems, including battery energy storage [12], and asynchronous motor or permanent magnet motor-based FESS [13], requires a full power converter, therefore, they could not provide the same power output as HIAC when equipped with converters of the same capacity.

At present, research on HIAC systems remains relatively limited. The seminal paper [14], by H. Akagi and H. Sato, was the first to propose a mechanical structure integrating DFMs with flywheel energy storage, along with active/reactive power decoupling control strategies. Li, et al. [15] conducted an in-depth control strategy analysis based on the state-space model of DFMs. Hu, et al. [16] developed a prototype of a motor arranged vertically and presented detailed experimental waveforms of

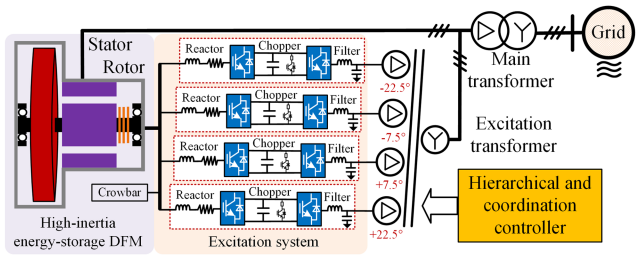

Fig. 1. Structure diagram of the HIAC system.

power control. However, these studies did not elaborate on the coordinated control strategies for integrating such equipment with grid voltage and frequency regulation, nor did they provide detailed research on strategies for active voltage and frequency support. Consequently, extant works are inadequate in terms of achieving effective grid inertia and reactive power support capabilities.

This article aims on enhancing the frequency and voltage stability of the grid with the proposed HIAC system, and the main contributions are as follows.

1) The proposed HIAC overcomes the shortcoming of insufficient inertia in conventional SynCon. High virtual inertia could be emulated by wide range speed varying, thereby reducing RoCoF of renewable energy dominated grids.
2) To meet the high active and reactive power output requirements and the wide slip rate for the HIAC, a high voltage, large capacity converter excitation system structure and its basic control methods are proposed.
3) A layered coordination control method is introduced to address the functional requirements and operational power constraints of the HIAC, ensuring its normal operation under various grid conditions.
4) A framework for actively providing voltage and frequency support by the HIAC to renewable energy plants is established. This framework effectively suppresses voltage and frequency fluctuations with very short response time.

The rest of this article is organized as follows. Section II introduces the principle and model of HIAC. Section III demonstrates the hierarchical and coordination control strategy of HIAC. Section IV presents the basic voltage and frequency support control strategy of HIAC. In Sections V and VI, the effectiveness and performance of the proposed HIAC are fully verified and tested by simulation and experimentation. Finally, Section VII concludes this article.

II. Principle and Model of the HIAC

A. Basic Structure of the HIAC System

The configuration of the HIAC system is illustrated in Fig. 1. It comprises a high-inertia energy-storage DFM, a high-voltage large-capacity excitation system, two transformers, protection systems (crowbar and dc-link chopper), and a hierarchical and coordination controller (HCC). The high-inertia energy-storage DFM is designed with low pole pairs to increase its maximum

speed and, thus, its capacity to store kinetic energy. In comparison with conventional DFM designs (mostly with $H < 1$ s), this energy-storage DFM employs a high-inertia rotor (exhibiting $H > 10$ s) to further enhance its energy-storage capacity. The high-inertia rotor can be attained through two methods: either by increasing the rotor size or by incorporating an additional flywheel. The excitation transformer adopts a phase-shift structure with four secondary windings, and the phase shifts are $\pm 22.5^\circ$, and $\pm 7.5^\circ$ for the four-channel parallel back-to-back (BTB) power converters. This configuration helps to eliminate current harmonic below 24th order [17], [18].

B. Basic Operating Principles of the HIAC

The operation of the HIAC is mainly controlled by the three-phase ac-excitation system, which could provide variable frequency and voltage excitation to the rotor winding. Consequently, the HIAC is able to operate within a large range of rotor speed, typically from 0.7 to 1.3 p.u. Based on the approximate voltage / frequency (V/F) ratio relationship between excitation voltage and rotor slip rate, the HIAC require only about 30% of the rated rotor voltage within this speed range. Consequently, under identical converter capacity conditions, the HIAC exhibit higher power output capabilities compared to STATCOMs.

By utilizing the power decoupling vector control method, the output active power and reactive power of the HIAC could be controlled independently. When the grid voltage undergoes fluctuations, the HIAC is able to swiftly adjust its output reactive power to mitigate these fluctuations. In instances where grid frequency undergoes fluctuations, the HIAC has the ability to release or absorb kinetic energy by adjusting its rotor speed, which increases the equivalent inertia of renewable energy stations, similar to a conventional SynCon. Hence, the HIAC could provide both swift transient voltage and frequency support to the grid and increase its stability.

C. Model of the High-Inertia Energy-Storage DFM

By utilizing the stator voltage-oriented vector control method, the d-axis and q-axis current of the DFM could be decoupled and controlled separately by the excitation system [19], the reactive power and active power can, thus, be controlled independently. Deriving from the flux equations of the DFM, the stator active power and reactive power can be expressed as

$$\begin{cases} P_s &= \frac{3}{2}U_s I_{sd} = \frac{3L_m}{2L_s}U_s I_{rd} \\ Q_s &= -\frac{3}{2}U_s I_{sq} = \frac{3U_s}{2\omega_s L_s}(U_s + \omega_s L_m I_{rq}). \end{cases} \tag{1}$$

The total output power of the DFM is the sum of the stator power and the rotor power, which could be expressed as

$$\begin{cases} P_t &= P_s + P_r = (1-s)P_s \\ Q_t &= Q_s + Q_r. \end{cases} \tag{2}$$

The rotor's mechanical equation utilizing the single-mass model could be expressed as

$$2H\frac{d\omega_r}{dt} = T_m - T_e - D\omega_r. \tag{3}$$

The kinetic energy released by the HIAC when adjusting its speed could be expressed as

$$E_k = \frac{1}{2}J\Delta\left(\frac{2\pi}{60}n\right)^2 = \frac{1}{2}J\Delta\Omega_r^2. \tag{4}$$

D. Model of the High-Voltage Large-Capacity Excitation System

1) Parallel Three-Level Neutral-Point-Clamped (3L-NPC) BTB Converter: The structure of the high-voltage large-capacity excitation system is illustrated in Fig. 2. The excitation system utilized several parallel connected BTB three-phase converters, each including a rotor-side converter (RSC) and a grid-side converter (GSC). The GSC is used to maintain a stable dc-link voltage, while the RSC is used to provide ac-excitation to the DFM. For HIAC systems with a capacity exceeding 10 MW, high dc-link voltage is required, this voltage is frequently selected to 5 kV or higher. Hence, a 3L-NPC converter is used as the GSC's topology [20], while a three-level active NPC is used as the RSC's topology to achieve better low-frequency performance.

For the HIAC system, higher single-unit capacity is required to suffice only a small number of units suffice to effectively support grid voltage and frequency regulation near wind farms. Furthermore, as the rotor overcurrent may occur during severe short-circuit faults, the excitation system requires larger current withstand capability. Hence, the excitation system employs multiple BTB converters in parallel, which enables the HIAC to output significantly more power and could also share the large fault current to ensure safe operation [21].

2) Basic Control Strategy of the BTB Converter: The GSC part of the BTB converter utilizes a grid voltage-oriented vector control scheme, with an inner current loop and a outer voltage loop to maintain the dc-link voltage. The reactive power of the GSC could also be controlled, but is normally set to zero. The RSC part employs the stator voltage-oriented vector control method, as previously mentioned. The inner current loop is utilized to regulate the d-axis and q-axis rotor current, while the outer loop can be configured as either a speed loop or a power loop. The control strategy is shown in Fig. 3. The switching between speed control and active power control will be discussed in Section III, while the detailed calculation of active power and reactive power reference will be provided in Section IV.

III. HCC OF THE HIAC

The HIAC system has a complex structure and numerous subsystems. The HCC plays a pivotal role in enabling the unit to effectively execute its frequency and voltage support functions, manage the state of charge (SOC), and ensure stable operation [22], [23].

A. Hierarchical Control of HIAC

As shown in Fig. 4, the hierarchical control structure can be categorized into three levels: primary control, secondary control, and tertiary control, according to their functions.

1) Primary Control: This level is responsible for the sampling of voltage and current. It also provides control of the

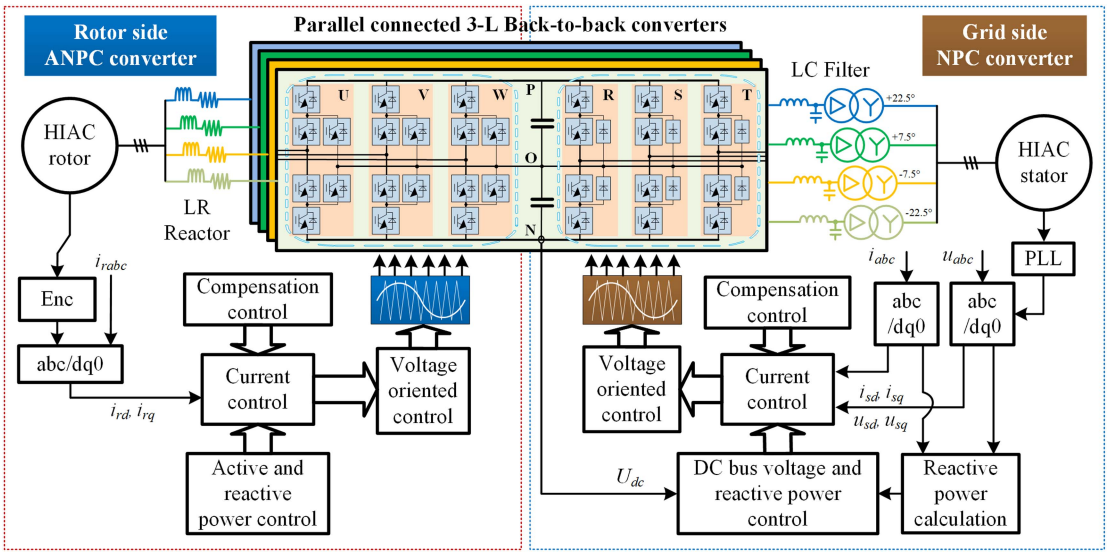

Fig. 2. Structure diagram of the high-voltage large-capacity excitation system.

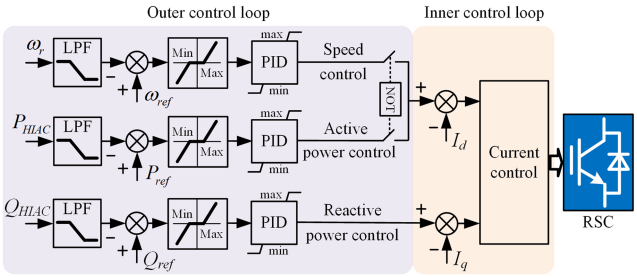

Fig. 3. Control strategy of the BTB converter.

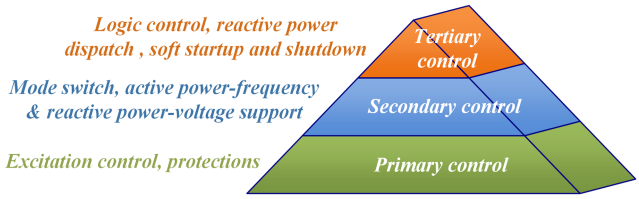

Fig. 4. Hierarchical control structure of HIAC.

TABLE I
RELATIONSHIP BETWEEN THE SOC AND SPEED OF THE HIAC

SOC	Over-discharge(OD)	Normal(N)	Overcharge(OC)
Speed range	$[n_{\min},n_{\text{lower}})$	$[n_{\text{lower}},n_{\text{upper}}]$	$(n_{\text{upper}},n_{\max}]$

TABLE II
CLASSIFICATION OF THE OPERATION MODES OF THE HIAC

Mode of the HIAC \ SOC of the HIAC	OD	N	OC
Speed limit mode	✓		✓
Condenser mode	✓	✓	✓
Hot standby mode		✓	
Frequency regulation mode		✓	
Condenser and frequency regulation mode		✓	
Speed recovery mode	✓		✓

current inner loop and power or speed outer loop, as well as various protective functions, such as overvoltage, overcurrent, dc bus chopper, and rotor winding crowbar operations. The basic control strategy presented above (see Fig. 3) belongs to this level.

2) Secondary Control: This level is mainly responsible for the active power-frequency and the reactive power-voltage support control of the HIAC, as well as the mode switch control to ensure that the HIAC is in normal operating condition. This level is the key to provide active inertia and voltage support.

3) Tertiary Control: This level is mainly responsible for logic control tasks within the HIAC, including soft start and shutdown, enabling/disabling active and reactive power control, and providing reactive power dispatching commands or steady-state target grid voltage signals. This level mainly interacts with the grid code and commands from the grid.

B. Coordination Control of HIAC

The rotor speed is indicative of the kinetic energy stored in the HIAC, and the SOC can be classified into three distinct states—normal, overcharge, and overdischarge—based on the interval in which the rotor speed is located, as provided in Table I. In the overcharge and overdischarge states, the HIAC will operate under a derated condition. Depending on the different functions of the HIAC, eight operating modes could be classified as shown in Table II. The coordination control of this section mainly belongs to the secondary control level in the hierarchical control.

1) Hot Standby Mode: In this mode, the SOC of the HIAC is in the normal state and is ready to provide voltage/frequency support to the renewable energy station. The RSC adopts a speed control strategy, in which the HIAC continuously absorbs a small amount of active power from the grid in order to overcome its

operating losses. The operating loss includes the friction and the conversion losses of the flywheel system. This ensures that the rotor speed is maintained at a set value.

2) Condenser Mode: In this mode, the RSC is still in speed control mode, and the HIAC rapidly adjusts the amplitude of the excitation current to suppress voltage fluctuations in the renewable energy station or adjust the output reactive power according to reactive power command. If the SOC of the HIAC is normal, the HCC controls the speed of the unit to maintain at the reference value; if the SOC of the HIAC is overcharge or overdischarge, the HCC switches the HIAC into the speed recovery mode. If there is a frequency drop event at this time, the HIAC switches into the condenser and frequency regulation mode to provide both reactive and active power support to the renewable energy station.

The voltage event can be determined by the absolute voltage deviation and also by commands from the tertiary control level. For example, the reactive power support starts when grid voltage falls under 0.95 p.u. [24]

3) Frequency Regulation Mode: In this mode, the SOC of the HIAC is normal, and the HCC switches the RSC to the power control mode. In the event of a frequency drop, the HIAC will release/absorb the corresponding active power according to instructions from the secondary control level in order to provide inertia support to the renewable energy station and suppress the frequency fluctuation.

The frequency drop event can be determined by the RoCoF and absolute frequency deviation. Active power support output is directly proportional to RoCoF, while the deadband for active power support is usually set at an absolute frequency deviation threshold (e.g., taking action when the frequency exceeds 100 mHz). [24]

Due to the high randomness of the frequency fluctuation, the HIAC will alternately be charging or discharging, which will cause the rotor to accelerate or decelerate repeatedly, resulting in the fluctuation of the rotational speed. If the HIAC enters the overcharge or overdischarge state due to a large speed variation, the HCC switches the HIAC into the speed limit mode. If the frequency event disappears, the HIAC returns back to the hot standby mode.

4) Condenser and Frequency Regulation Mode: The different between this mode and the frequency regulation mode is that the HIAC is required to deliver both reactive and active support to the renewable energy station in order to mitigate voltage and frequency fluctuations concurrently. Except the reactive power-voltage control function, the control logic in this mode is same as in the frequency regulation mode. The judgment of events is same as above.

5) Speed Limit Mode: When providing active power support to the renewable energy station, the rotor speed of the HIAC will vary in a wide range. Due to the mechanical strength of the rotor and the maximum slip rate limitation, the rotor speed of the HIAC should be constrained within the upper and lower limits in order to ensure safe operation. In order to prevent the rotor speed from exceeding the upper and lower limits due to long-time charging and discharging, the HCC will switch the HIAC into the speed limit mode after the SOC enters overcharge or overdischarge state, and restricts the charging and discharging power. The detailed control logic is as follows.

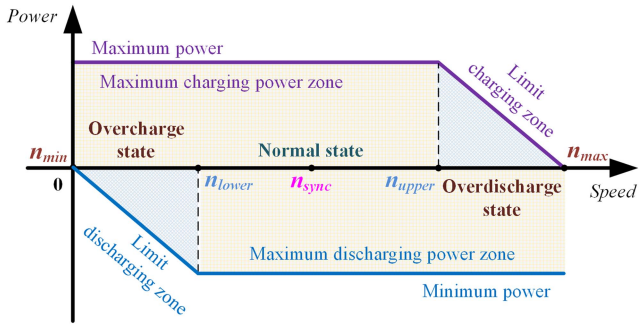

Fig. 5. Power constraint of the HIAC within different speed intervals.

When the SOC is in overcharge state, i.e., $n_{\text{upper}}<n\leq n_{\max}$, to prevent the rotor speed from exceeding the maximum value, the maximum charging power of the HIAC will be constrained. As the speed increases, the maximum charging power is reduced linearly until it reaches zero, at which point the HIAC is prohibited from charging. However, the discharge power is not constrained and the HIAC can still provide output power-frequency support control to the renewable energy station with maximum discharge power. The aforementioned scenario is inverted when the SOC is in an overdischarge state, i.e., $n_{\text{upper}}>n\geq n_{\max}$, resulting in the discharge power being constrained.

The charging and discharging power constraint functions of the HIAC at different rotor speed can be expressed as

$$P_{\text{max\_}c}=\begin{cases}P_{\max} & ,\ n_{\min}\leq n\leq n_{\text{upper}}\\ \frac{-P_{\max}}{n_{\max}-n_{\text{upper}}}(n-n_{\max}) & ,\ n_{\text{upper}}<n\leq n_{\max}\end{cases} \tag{5}$$

$$P_{\text{max\_dc}}=\begin{cases}-P_{\max} & ,\ n_{\text{lower}}\leq n\leq n_{\max}\\ \frac{-P_{\max}}{n_{\text{lower}}-n_{\min}}(n-n_{\min}) & ,\ n_{\min}\leq n<n_{\text{lower}}.\end{cases} \tag{6}$$

To provide a clear visualization of the above equations, the HIAC power limitation curve as a function of rotor speed variation is illustrated in Fig. 5.

6) Speed Recovery Mode: When the SOC of the HIAC is overcharge or overdischarge, and the frequency event of the renewable energy station disappears, the HCC will switch the HIAC into the speed recovery mode. In this mode, the HIAC absorb or release active power in order to gradually restore the speed to the original reference value. Following this, the HIAC will switch back to hot standby mode. In order to avoid the charging and discharging process of the HIAC leading to another drop or increase in the grid frequency, it is necessary to take into account both the SOC state and the grid frequency. Hence, the HCC need to adjust the power constraint of the HIAC to appropriately control the rate of speed recovery. The detailed control logic in speed recovery mode is as follows.

When the SOC is in overcharge state, if the system frequency deviation $\Delta f\leq\Delta f_{\text{set}}$, where $\Delta f=f_g-f_0$, the HIAC discharges at a constant power, and the rotor speed is gradually reduced. If $\Delta f_{\text{set}}<\Delta f\leq\Delta f_{\max}$, the HIAC's discharge power

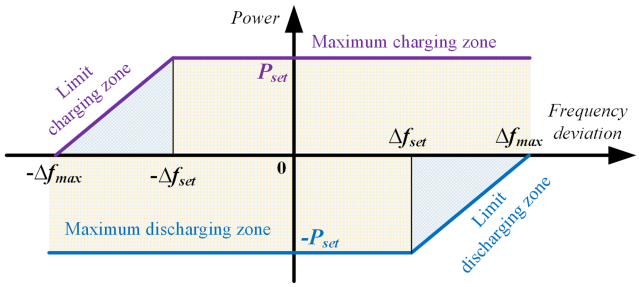

Fig. 6. Power constraint of the HIAC within different frequency deviation intervals.

is constrained, and the power is inversely proportional to the frequency deviation. When $\Delta f > \Delta f_{\max}$, the HIAC is prohibited from discharging. During the speed recovery, if the grid frequency suddenly increases, the HCC blocks the recovery process. The discharge power constraint of the HIAC at different frequency deviation ranges is shown in the following equation:

$$P_{\mathrm{dc}}=\begin{cases}-P_{\mathrm{set}} & ,\ \Delta f \le \Delta f_{\mathrm{set}} \\ \frac{P_{\mathrm{set}}}{\Delta f_{\max}-\Delta f_{\mathrm{set}}}(\Delta f-\Delta f_{\max}) & ,\ \Delta f_{\mathrm{set}} < \Delta f \le \Delta f_{\max} \\ 0 & ,\ \Delta f_{\max} < \Delta f.\end{cases} \tag{7}$$

When the SOC is in overdischarge state, the aforementioned scenario is inverted, and the charge power constraint be expressed as

$$P_{c}=\begin{cases}P_{\mathrm{set}} & ,\ -\Delta f \le \Delta f_{\mathrm{set}} \\ \frac{P_{\mathrm{set}}}{\Delta f_{\max}-\Delta f_{\mathrm{set}}}(\Delta f+\Delta f_{\max}) & ,\ -\Delta f_{\mathrm{set}} < \Delta f \le -\Delta f_{\max} \\ 0 & ,\ \Delta f < -\Delta f_{\max}.\end{cases} \tag{8}$$

The curve of power constraint versus the frequency deviation is illustrated in Fig. 6.

7) Coordination Control Conclusion: According to frequency/voltage support demands of the renewable station and the different SOC of the HIAC, the HCC will frequently switching the operation modes. According to the previous 6 modes, the mode switching logic of the HCC is concluded in Fig. 7.

In Fig. 7, the definitions of voltage/frequency events are as described above in different operation modes. The steady state of station means all the fault events are cleared, both the frequency and voltage of the grid are in their normal states. The normal state of the SOC means the rotor speed is within $[n_{\mathrm{lower}}, n_{\mathrm{upper}}]$.

IV. Active Voltage and Frequency Support Control Strategy of the HIAC

The reactive power-voltage and active power-frequency control functions of HIAC are mainly implemented by the secondary control level of HCC. When a voltage or frequency event occurs in the renewable energy station, the HCC will actively adjust the reactive or active power of the HIAC in order to achieve suppression of voltage and frequency fluctuations.

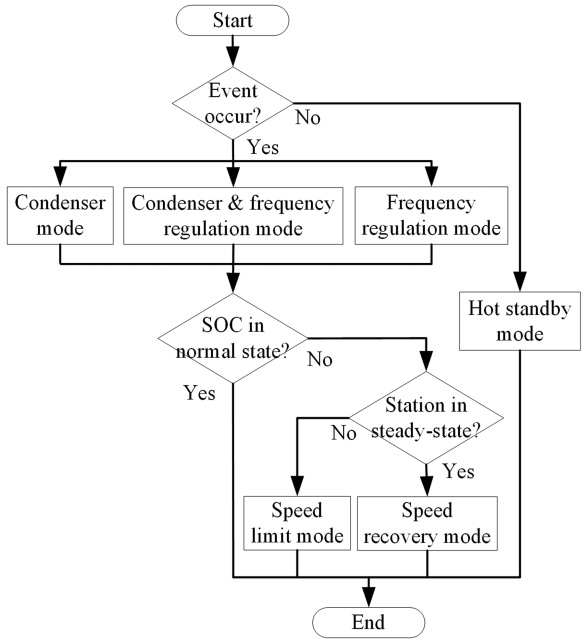

Fig. 7. Mode switching logic of the HCC.

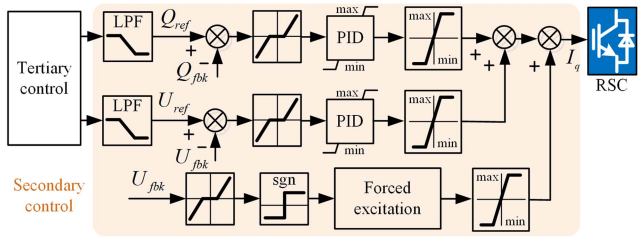

Fig. 8. Reactive power-voltage support control of the HIAC.

A. Reactive Power-Voltage Support Control Strategy

The reactive-voltage support control block diagram of the HIAC is shown in Fig. 7. The reactive-voltage support control of HIAC is divided into the following three levels according to the different time scales.

1) 10 ms Scale: In the event of a short-circuit fault resulting in a significant voltage drop (for example, the voltage falling to below 50% of the rated value), the HCC instantaneously increases the excitation current to the maximum permissible level (i.e., forced excitation). As a result, the HIAC could provide a swift and strong reactive power support to the grid, thereby preventing the voltage collapse and helping the voltage recovery.

As demonstrated in Fig. 8, the forced excitation control exhibits operational characteristics similar to bang–bang control, marked by rapid state transitions. Nevertheless, this method requires fast real-time grid voltage monitoring for the purpose of fault detection. In contrast to conventional dc excited SynCons, ac-excitation configurations achieve superior performance through high-voltage dc bus, enabling rapid increase of rotor current that reduces the overall response latency to around tens of milliseconds under transient conditions.

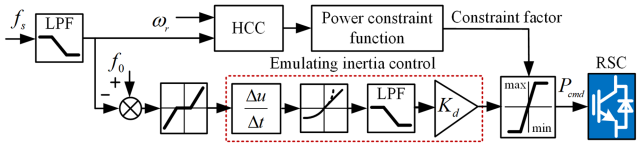

Fig. 9. Active power-frequency support control of the HIAC.

2) 100 ms Scale: When sudden grid load changes result in overvoltage or voltage fluctuations, the secondary control level system utilities grid voltage feedback to adjust the HIAC's reactive power, thereby suppressing voltage fluctuations. The voltage controller utilizes a proportional integral (PI) controller, hence forming a dual-loop control. Considering the low-pass filter (LPF) of the grid voltage, the overall response speed may be delayed to around 100 ms scale.

3) 1000 ms Scale: According to the reactive power instructions given by the electricity system operator, the HCC adjusts the reactive power of the HIAC accordingly, in order to satisfy the demand for reactive power in the grid or to adjust the steady-state voltage level of the system. As the reactive power reference command is from remote voltage control stations, the communication delay is around 1000 ms scale.

The integration of reactive power support control across the aforementioned three time scales enables HIAC to provide voltage support in a rapid and spontaneous manner during instances of short-circuit faults and voltage fluctuations. In addition, it is capable of generating reactive power values that are in accordance with grid commands.

B. Active Power-Frequency Support Control Strategy

The active power-frequency support control block diagram of the HIAC is shown in Fig. 9. The implementation of the virtual inertia control algorithm enables the HIAC to couple the output active power with the grid frequency, thereby enhancing the equivalent inertia of the system. Specifically, in instances of frequency increase, the inertia controller immediately increases the active power reference, prompting the HIAC to transition into the charging state. Concurrently, the DFM absorbs energy and mitigates the system frequency increase. Conversely, in the event of a frequency drop, the HIAC transitions to a discharging state, thereby providing energy to the grid and ensuring that grid frequency remains within the normal range.

During frequency disturbances, the conventional SynCon provides active power to the grid under the combined effect of its mechanical inertia and damper winding. The rotor speed of the SynCon is approximately a second-order delay relationship to the grid frequency [25]. To mimic this behavior, a second-order LPF with a derivative term is connected in series. The derivative term generates the power reference, while the LPF filters the input signal and simulates the SynCon rotor's response to grid-frequency change. The transfer function could be expressed as

$$G_i(\mathcal{S}) = \frac{\omega_n^2 K_d \mathcal{S}}{\mathcal{S}^2 + 2\omega_n \xi \mathcal{S} + \omega_n^2}. \tag{9}$$

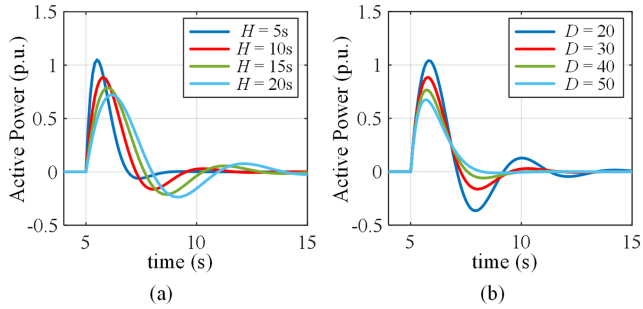

Fig. 10. Inertial response of the virtual inertia control with (a) different inertia constant and (b) different damper constant. (a) $D = 30$. (b) $H = 10$ s.

The transfer function of the SynCon's rotor speed to the grid frequency could be approximately expressed as [25]

$$G_{sc}(\mathcal{S}) = \frac{1}{2HX_s\mathcal{S}^2 + DX_s\mathcal{S} + 1}. \tag{10}$$

From (9) and (10), the LPF's parameters could be calculated by the desired inertia and damper constant, while the inertia gain K_d could be used to furthur adjust the active power response of the HIAC without affecting the damping ratio. For simplicity, the stator impedance X_s is chosen to 1.0, which is a common value for conventional SynCons, hence, the LPF's parameters could be calculated as

$$\begin{cases} \omega_n = \sqrt{\frac{1}{2H}} \\ \xi = \frac{D\omega_n}{2}. \end{cases} \tag{11}$$

The inertial response characteristics of the proposed HIAC under varying inertia constant H and damping constant D are analyzed in Fig. 10. As illustrated, increasing the inertia constant extends the duration of active power support during transient events, while reducing the damping constant enhances the peak active power but also suffers from longer oscillations. From the perspective of facilitating parameter tuning, a better strategy is to first set appropriate values for H and D to achieve the desired damping ratio and support duration, and then adjust the active power support capability by tuning the value of K_d. This parameter tuning approach will be adopted in the subsequent analysis of this article.

Apart from the virtual inertia, the power constraint function from the HCC controller also affects the inertial response of the HIAC, as presented in Section III. The power constraint guarantees that the output active power of the HIAC undergoes a gradual decline to zero in the overdischarge state, thus preventing a secondary frequency drop.

V. Simulation Results and Analysis

A. Simulation Setup

To evaluate the reactive voltage and active frequency support characteristics of the HIAC, a detailed simulation model of the renewable energy station is built in the MATLAB/Simulink platform, as shown in Fig. 11. The renewable energy station includes a 100 MW wind farm, a 100 MW photovoltaic plant, a 100 MW hydroelectric unit, a 100 MW thermal unit and an HIAC

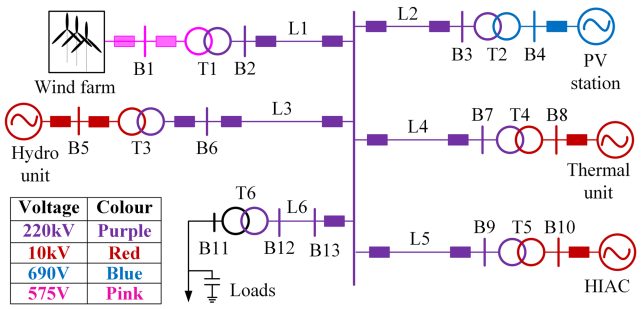

Fig. 11. Detailed structure of the renewable energy station.

TABLE III
SIMULATION PARAMETERS OF THE HIAC

Para.	Value	Para.	Value	Para.	Value
S_n	11.1 MVA	U_s	10.5 kV	U_r	9.3 kV
P_{max}	30 MW	p	2	U_{dc}	5 kV
E	112 MJ	J	9591 kg·m^2	H	10.7s
R_s	0.02 Ω	R_r	0.01 Ω	L_m	45.8 mH
L_{sl}	0.66 mH	L_{rl}	0.92 mH	N	1.13:1
s_{nom}	± 0.25	n_{lower}	1125 rpm	n_{upper}	1875 r/min
s_{max}	± 0.3	n_{min}	1050 rpm	n_{max}	1950 r/min

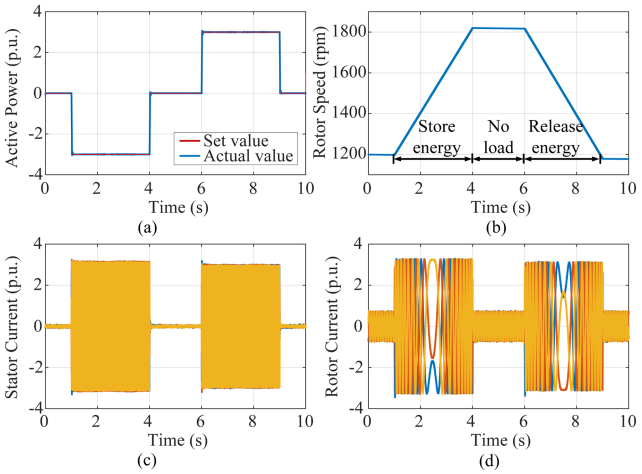

Fig. 12. Response of the HIAC under step change of active power command. (a) Active power response. (b) Speed response. (c) Stator current response. (d) Rotor current response.

deployed on a 35 kV bus. The main simulation parameters of the HIAC are shown in Table III. Three sets of simulations, including a stand-alone power response simulation, a grid-connected steady-state simulation and a short-circuit fault simulation, are carried out to verify the frequency and voltage support capability of the HIAC for the renewable energy station.

B. Stand-Alone Power Response Evaluation

1) Step Active Power Response: In the first case, a step power command response of the HIAC in stand-alone operation is tested. An ideal three-phase voltage power source with internal impedance is used to simulate the grid. The waveform of the HIAC with active power command step change is illustrated in Fig. 12. The initial rotor speed of the HIAC is set to 0.8 p.u. The

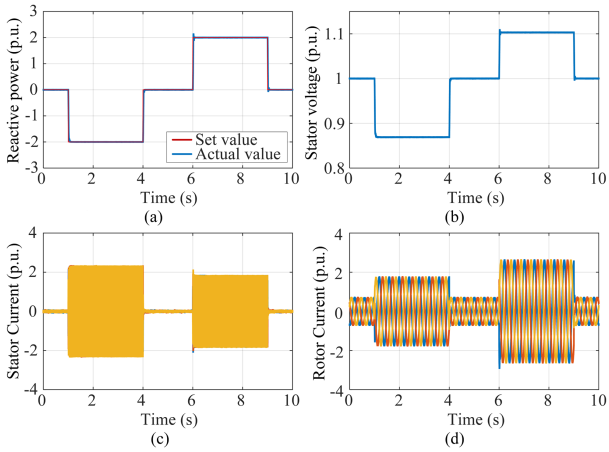

Fig. 13. Responses of the HIAC under step change of reactive power command. (a) Reactive power response. (b) Stator voltage response. (c) Stator current response. (d) Rotor current response.

active power command is changed from 0 to 3 p.u. at $t = 1$ s and from 0 to -3 p.u. at $t = 6$ s. As shown in Fig. 12(a), the active power follows its command swiftly with no steady-state error. In Fig. 12(b), the rotor speed rises from 0.8 p.u. to around 1.2 p.u., storing energy, and declines back to 0.8 p.u., releasing energy to the grid. Hence, the HIAC could provide bidirectional energy storage capacity for the grid.

2) Step Reactive Power Response: In this case, a step reactive power command response of the HIAC in stand-alone operation is tested. The waveform of the HIAC with reactive power command step change is illustrated in Fig. 13, with the rotor speed set to a fixed 0.95 p.u. As shown in Fig. 13(a), the reactive power could also follow its command swiftly, both inductive and capacitive reactive power command. As a result, the HIAC could provide voltage support to the grid by swiftly adjusting its output reactive power.

C. Inertia and Voltage Support Evaluation in an Ideal Grid

1) Inertia Support: In this scenario, the inertia support capability of the HIAC is presented, and its performance is compared with that of a conventional 10 Mvar SynCon. An ideal three-phase voltage power source is used to simulate the grid., while a frequency step change is set at 10 s of the simulation, from 1.0 p.u. (50 Hz) to 0.996 p.u. (49.8 Hz). The HIAC's virtual inertia loop is set to $H = 10$ s and $D = 30$, with a range of K_d values being tested.

The inertial response waveforms of the HIAC and SynCon are compared in Fig. 14. As demonstrated, the HIAC with $K_d = 10$ achieves comparable active power contribution to a conventional SynCon with $H = 100$ s. With $K_d = 15$, the peak active power could be further increased to nearly 3.0 p.u. During frequency transients, the HIAC rotor speed decreases to 0.83 p.u., effectively releasing more kinetic energy than SynCon systems where rotor speed remains fixed at grid frequency. This allows the HIAC to realize equivalent inertia values exceeding 100 s, which is 10 times higher than conventional SynCons with identical mechanical inertia parameters.

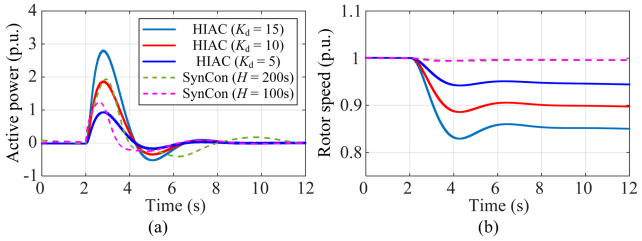

Fig. 14. Response of the HIAC and SynCon with different inertia constant. (a) Active power response. (b) Rotor speed response.

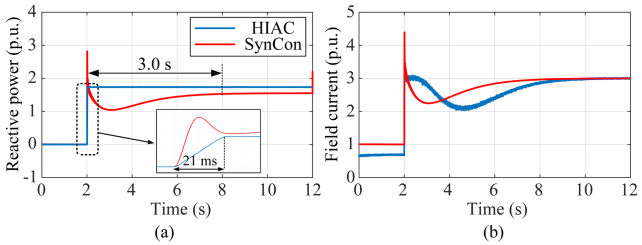

Fig. 15. Response of the HIAC and SynCon under a grid-voltage drop event. (a) Reactive power response. (b) Field current response.

2) Voltage Support: In this scenario, the voltage support capability (forced excitation) of the HIAC is compared with the 10 Mvar SynCon. A grid voltage step change is set at 10 s of the simulation, from 1.0 to 0.7 p.u. The maximum dc excitation voltage of the SynCon is set to 5 p.u., while the maximum field current of both condensers are set to 3.0 p.u. It is noteworthy that oscillating terms are eliminated in the waveforms by a notch filter to clearly show the fundamental term.

As shown in Fig. 15, both the HIAC and SynCon have the capacity to deliver high-reactive power ($>$ 1.5 p.u.) to the grid during the event. In consideration of the inherent properties of dc excitation, the SynCon has the capacity to deliver pulse reactive power during transient periods. However, it should be noted that the pulse period is of a very brief duration. Subsequent to the pulse response, a delay of approximately 3 s is observed before the SynCon attains its maximum reactive output power. For the HIAC, though in the absence of initial pulse support, the maximum reactive power could be achieved within 21 ms, which is significantly faster than the SynCon. Consequently, the HIAC has the potential to provide strong and rapid voltage support to the grid during short-circuit faults.

D. Evaluation of Renewable Energy Station Support Capability

In this case, various disturbance scenarios within the renewable energy station are modeled to assess the frequency and voltage support capabilities of the HIAC.

1) Wind Speed Disturbance: In the first scenario, a wind speed disturbance is introduced within the wind farm to evaluate the HIAC's effectiveness in suppressing frequency fluctuations. A sudden wind speed fluctuation disrupts the wind farm's power control loop, inducing active power variations [as shown in Fig. 16(a)]. With the HIAC activated, its output active power compensates for the wind farm's power fluctuations [depicted in Fig. 16(c)], enabling faster frequency recovery and effectively dampening frequency oscillations. Compared to a conventional SynCon, the HIAC demonstrates superior inertial support by fully leveraging its rotor kinetic energy. Specifically, the maximum frequency deviation is limited to approximately 0.0025 p.u. with the HIAC, whereas a SynCon with $H = 100$ s exhibits a larger deviation of 0.0035 p.u. These results validate the HIAC's enhanced frequency support capability relative to conventional SynCons.

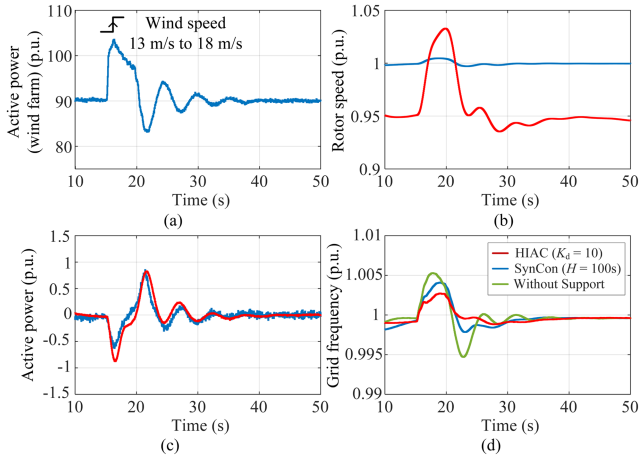

Fig. 16. Response of the HIAC and SynCon under a wind speed disturbance. (a) Active power of wind farm. (b) Rotor speed response. (c) Active power response. (d) Grid frequency response.

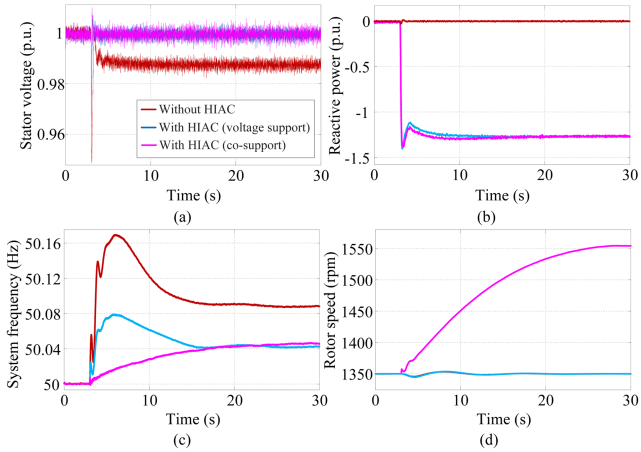

Fig. 17. Response of the HIAC with a reactive load step. (a) Stator voltage of the HIAC. (b) Reactive power of the HIAC. (c) System frequency. (d) Rotor speed of the HIAC.

2) Reactive Load Disturbance: In the second scenario, a 30 Mvar reactive load step is implemented in the simulation to evaluate the voltage support capabilities of the HIAC. The waveforms depicting the system's performance without the HIAC, with the HIAC's voltage support function, and with the combined frequency and voltage support function are illustrated in Fig. 17. When the HIAC is engaged in providing voltage support to the grid, the steady-state system voltage is sustained at 1 p.u.; conversely, in the absence of the HIAC, the voltage

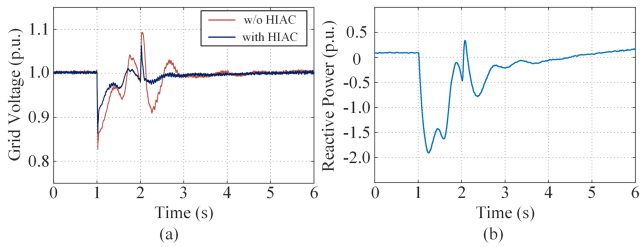

Fig. 18. Response of the HIAC with a remote short-circuit fault. (a) Grid voltage. (b) Reactive power of the HIAC.

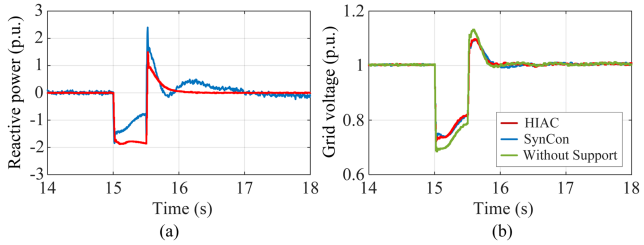

Fig. 19. Response of the HIAC with a local short-circuit fault. (a) Reactive power response. (b) Grid voltage response.

decreases to 0.99 p.u. In addition, the steady-state system frequency experiences a decline from 50.08 to 50.04 Hz when the HIAC offers cosupport. Therefore, it can be concluded that the HIAC is capable of delivering both frequency and voltage support to the renewable energy station during complex grid disturbances.

3) Short-Circuit Fault Support: Short-circuit faults are extremely harmful to the safe operation of renewable energy station. Consequently, the performance of the HIAC is evaluated under conditions of three-phase symmetric short-circuit faults in the third scenario. To simulate both remote and local short-circuit faults, a variable grounding resistance is implemented on the 220 kV bus.

When the remote short-circuit fault is triggered, the waveforms of the HIAC are shown in Fig. 18. The fault is activated at $t = 1$ s and is cleared at $t = 2$ s. During this fault event, the minimum grid voltage decreases to 0.82 p.u. in the absence of the HIAC, whereas it rises to 0.86 p.u. with the HIAC in operation. The reactive power output of the HIAC is mainly controlled by the grid voltage feedback loop depicted in Fig. 8. Through the implementation of voltage feedback control, the HIAC is capable of both raising the voltage nadir and mitigating voltage fluctuations following the fault.

When the local short-circuit fault is triggered, the grid voltage falls to a lower level at around 0.7 p.u., as shown in Fig. 19. In this scenario, the HIAC activates its forced excitation mode, rapidly increasing the rotor current to its maximum capacity in order to provide transient voltage support. Consequently, the HIAC is able to deliver substantial reactive power support even during severe short-circuit faults. However, it is important to note that the maximum output reactive power may be limited due to the constraints of the RSC capacity.

As shown in Fig. 19, under the same maximum excitation current constraint, the HIAC delivers higher reactive power (1.9 p.u.) compared to a conventional SynCon. It maintains peak

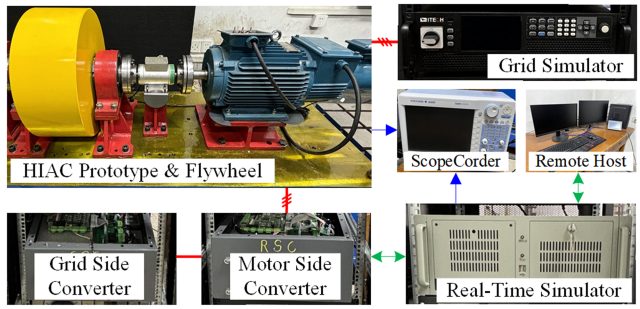

Fig. 20. Setup of the HIAC prototype platform.

reactive power output throughout the fault duration and the reactive power restores to zero faster than the SynCon, highlighting the superior power regulation capability of ac excitation. Consequently, the grid voltage nadir rises from 0.7 to 0.75 p.u., directly validating the HIAC's voltage support performance.

E. Implications for Component Design Constraints

As demonstrated by the results of the above simulation, it can be concluded that the HIAC exhibits significant performance enhancements relative to traditional SynCons. The performance characteristics of the system impose distinct implications for overall system design constraints, encompassing two key dimensions: implications with respect to motor design and considerations regarding exciter design.

In the context of the DFM design, the reduction in H requirement has the effect of relaxing mechanical design constraints (e.g., rotor material strength) in comparison with conventional SynCons, thereby enabling the creation of more compact structures. However, the wide speed regulation range ($\pm$ 30%) introduces new demands, such as the necessity for rotor windings to withstand higher excitation voltage during speed changes, and the requirement for the total loss of the DFM to be further optimized in order to match conventional SynCon.

In the context of converter design, the HIAC's prolonged operation near synchronous speed necessitates refined thermal management and modulation strategies. More critically, during severe grid faults, the converter must tolerate fault currents while ensuring its thermal stress remains strictly within safe limits.

VI. Experimental Results and Analysis

A. Experimental Platform Setup

The characteristics of the HIAC are tested on a prototype platform, which included a DFM and an additional coaxial flywheel. The experimental platform setup is shown in Fig. 20. Both the RSC and the GSC utilize an IGBT-based 3L-NPC inverter, and an Itech IT7900 grid simulator is used to simulate the grid. The proposed control method is implemented on the Simulink real-time simulation platform, and a real-time simulator is used to control the RSC based on the Simulink model. The detailed parameters of the ac SynCon prototype are provided in Table IV, all rotor side values are converted to the stator side.

During the experiments, the currents and voltages were measured using isolated sensors, equipped with a 5 kHz LPF to

TABLE IV
PARAMETERS OF THE HIAC PROTOTYPE

Para.	Value	Para.	Value	Para.	Value
S_n	5.5 kVA	U_s	380 V	U_{dc}	100 V
J	≈1.5 kg·m^2	p	2	s_{max}	± 0.3
R_s	1.004 Ω	R_r	1.078 Ω	L_m	193.5 mH
L_{sl}	6.61 mH	L_{rl}	11.86 mH	N	18:7

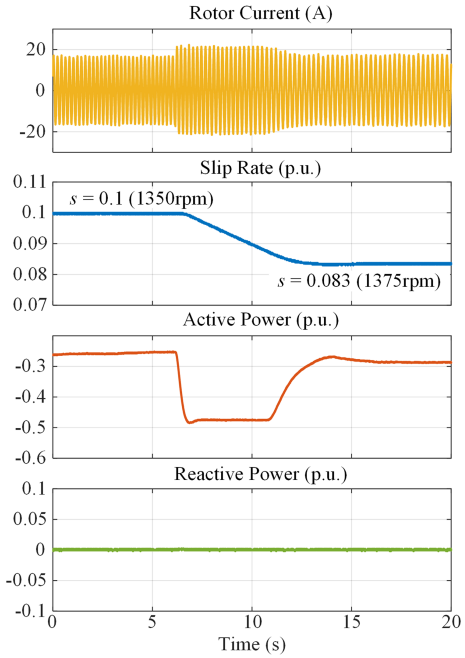

Fig. 21. Waveforms of the HIAC in the hot standby mode.

eliminate high-frequency noises. Other variables, including active power, reactive power and grid frequency were computed and filtered within the real-time simulator, and output through DAC channels. This setup allowed for precise monitoring and analysis of the HIAC's performance.

B. Experimental Verification

1) Hot Standby Mode Test: In the first experiment, the hot standby mode of the HIAC is tested. The HCC will maintain the HIAC's speed at the desired rotor speed, absorbing a small amount of active power from the grid. The resulting waveforms are shown in Fig. 21. The rotor speed reference is initially set at 1350 r/min and subsequently adjusted to 1375 r/min. As shown in the figure, the rotor speed follows the command swiftly, while the reactive power remains at 0 p.u. during the hot standby mode.

2) Step and Ramp Power Response Test: In the second experiment, the response of the HIAC to different power commands is evaluated. Under normal SOC conditions, the power command is unconstrained. Conversely, when the SOC deviates from normal levels, the power command will be decreased linearly in relation to the rotor speed by the HCC. Consequently, both a step power command and a ramp power command are employed in the testing, with the ramp power command designed to simulate conditions in which the HIAC is in overcharge or overdischarge states. The waveforms of the HIAC at subsynchronous speed

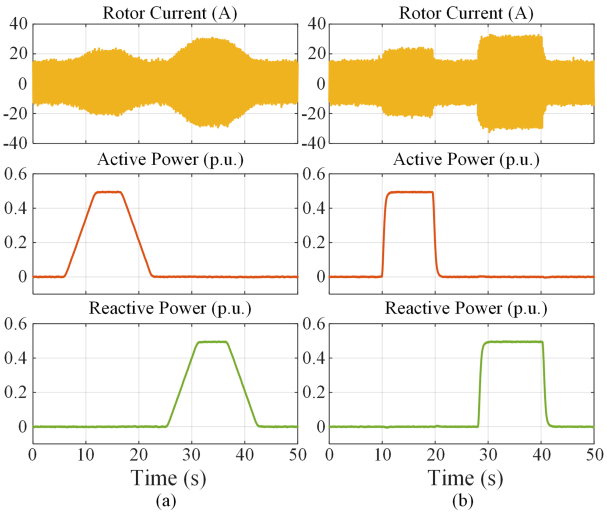

Fig. 22. Waveforms of the HIAC's power response at subsynchronous speed.

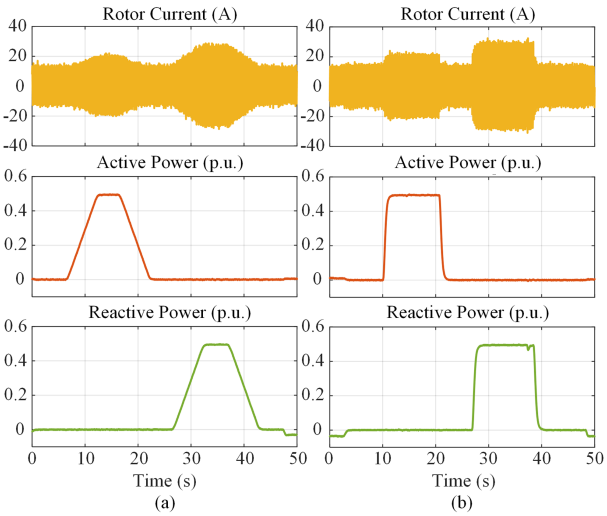

Fig. 23. Waveforms of the HIAC's power response at super-synchronous speed.

and super-synchronous speed are illustrated in Figs. 22 and 23, respectively. The figures demonstrate that the HIAC is capable of following step and ramp power commands at both subsynchronous and super-synchronous speeds.

3) Inertia Support Test: In the third experiment, the response of the HIAC during a frequency disturbance is evaluated. The inertia constant H is set to 10, the damper constant is set to 30, which is equivalent to the value employed in the simulation section. However, the inertia gain K_d is set to 2 due to the limited active power absorbing capability of the grid simulator.

As illustrated in Fig. 24(a), the grid frequency is reduced to 0.98 p.u., while the HIAC increases its output active power to 0.2 p.u. peak. In Fig. 24(b), the frequency decline is further diminished to 0.96 p.u., accompanied by an augmentation in active power to 0.4 p.u. The results indicate that the proposed HIAC has the capability to automatically provide inertial support that is analogous to conventional SynCon during frequency disturbances.

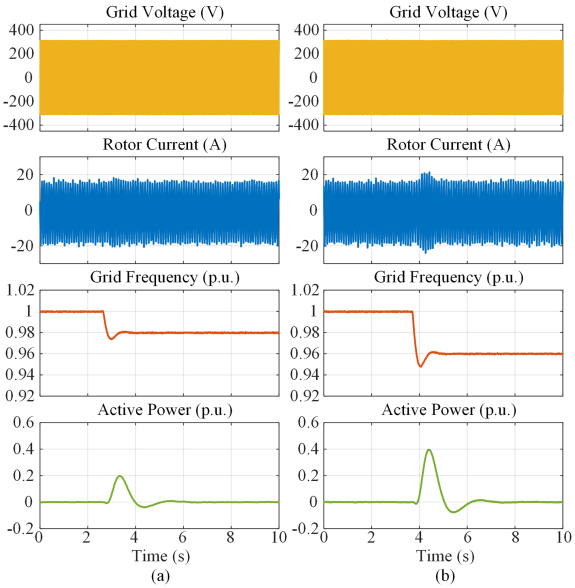

Fig. 24. Waveforms of the HIAC's power response with a grid frequency drop. (a) To 0.98 p.u. (b) To 0.96 p.u.

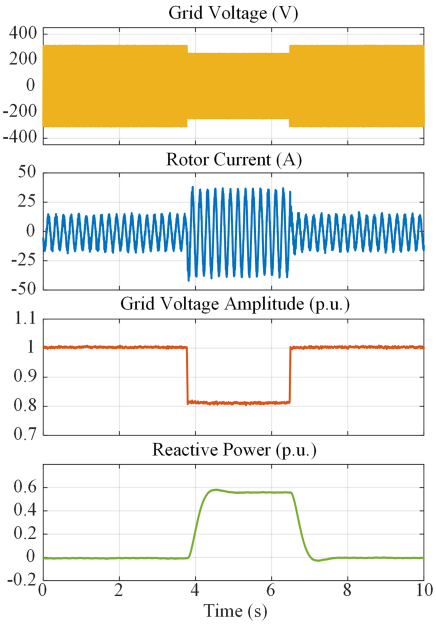

Fig. 25. Waveforms of the HIAC's power response with a grid voltage drop to 0.8 p.u.

4) Voltage Support Test: In the last experiment, the HIAC's response during voltage disturbances was evaluated. The forced excitation threshold has been set to 0.85 p.u. of the grid voltage amplitude, and the maximum rotor current has been set to 1 p.u. (≈ 31 A) due to the limited capacity of the experimental platform. The rotor speed is fixed to 1350 r/min ($s = 0.1$).

As illustrated in Fig. 25, the grid voltage is reduced to 0.8 p.u., thereby initiating the forced excitation. Consequently, the rotor current instantaneously increases to 1 p.u., thereby facilitating the provision of reactive power support to the grid. It is important to note that the reactive power calculated by the power meter is subject to a delay, which can be attributed to its LPF. Conversely, the actual voltage support is characterized by its rapid response, which is evident as the rotor current increases in a corresponding manner.

VII. Conclusion

This article presents an HIAC that exhibits robust capabilities in reactive power-voltage and active power-frequency support, addressing several limitations associated with the traditional SynCon. The HIAC is designed to deliver virtual inertia, as well as rapid active and reactive power support to the grid, thereby suppressing voltage and frequency fluctuations in renewable energy stations.

1) By utilizing the ac excitation and the inertia emulation method, the HIAC could effectively leverage the kinetic energy stored in the rotor. This approach has been shown to yield an equivalent inertia that is more than 10 times greater than that of the conventional SynCon with same mechanical inertia.
2) The voltage support strategy combining different time scales could provide rapid reactive power support to the grid with a response time of around 20 ms. The parallel B2B converter guarantees adequate excitation capacity ($\approx$ 3 p.u.).
3) The HCC controller allows the HIAC to transit between different operational modes in response to variations in SOC and various grid faults. This ensures the maintenance of fully controllable and stable operation of the HIAC under all grid scenarios.

To further enhance the HIAC's performance, potential improvements include adopting the magnetic bearing structure and developing modular design schemes. Optimization of the DFM's electromagnetic design and the integration of low-voltage ride through strategies with the proposed HCC controller will also be studied in future researches.

References

[1] J. Wang, J. Zhang, Q. Hou, and N. Zhang, "Synchronous condenser placement for multiple HVDC power systems considering short-circuit ratio requirements," *IEEE Trans. Power Syst.*, vol. 40, no. 1, pp. 765–779, Jan. 2025.
[2] S. Ghimire, K. Vatta Kkuni, E. D. Guest, K. H. Jensen, and G. Yang, "Impact of synchronous condensers on small-signal stability of offshore wind power plants," *IEEE Access*, vol. 12, pp. 168018–168029, 2024.
[3] S. Hadavi, N. Mohammed, A. Mehrizi-Sani, and B. Bahrani, "Quantifying stability in inverter-based weak grids in the presence of synchronous condensers," *IEEE Open Access J. Power Energy*, vol. 11, pp. 314–324, 2024.
[4] X. Liu, H. Xin, D. Zheng, D. Chen, and J. Tu, "Transient stability of synchronous condenser co-located with renewable power plants," *IEEE Trans. Power Syst.*, vol. 39, no. 1, pp. 2030–2041, Jan. 2024.
[5] H. Li, C. Nie, and F. Wang, "Grid strengthening IBR: An inverter-based resource enhanced by a co-located synchronous condenser for high over-current capability," *IEEE Open J. Power Electron.*, vol. 3, pp. 535–548, 2022.
[6] S. Hadavi, D. B. Rathnayake, G. Jayasinghe, A. Mehrizi-Sani, and B. Bahrani, "A robust exciter controller design for synchronous condensers in weak grids," *IEEE Trans. Power Syst.*, vol. 37, no. 3, pp. 1857–1867, May 2022.
[7] F. Palone, F. M. Gatta, A. Geri, S. Lauria, and M. Maccioni, "New synchronous condenser–flywheel systems for a decarbonized Sardinian power system," in *Proc. IEEE Milan PowerTech*, 2019, pp. 1–6.

[8] L. Hiquiana, J. Sun, J. Schmall, and S. Zuloaga, "Interactions between wind turbines and synchronous condensers equipped with flywheels," in *Proc. 9th IEEE Workshop Electron. Grid*, 2024, pp. 1–6.
[9] M. Caldora et al., "Synchronous condensers with flywheel for power systems with high penetration of res: The case of italian transmission grid," in *Proc. AEIT Int. Annu. Conf.*, 2022, pp. 1–5.
[10] Y. Chen, W. Xu, Y. Liu, Z. Bao, Z. Mao, and E. M. Rashad, "Modeling and transient response analysis of doubly-FED variable speed pumped storage unit in pumping mode," *IEEE Trans. Ind. Electron.*, vol. 70, no. 10, pp. 9935–9947, Oct. 2023.
[11] A. Gonzalo, L. Jesús, R. Miguel, M. Luis, and I. Grzegorz, *Doubly Fed Induction Machine: Modeling and Control for Wind Energy Generation Applications*. Berlin, Germany: Wiley, 2011.
[12] X. Li, D. Hui, and X. Lai, "Battery energy storage station (BESS)-based smoothing control of photovoltaic (PV) and wind power generation fluctuations," *IEEE Trans. Sustain. Energy*, vol. 4, no. 2, pp. 464–473, Apr. 2013.
[13] S. Ghosh and S. Kamalasadan, "An integrated dynamic modeling and adaptive controller approach for flywheel augmented DFIG based wind system," *IEEE Trans. Power Syst.*, vol. 32, no. 3, pp. 2161–2171, May 2017.
[14] H. Akagi and H. Sato, "Control and performance of a doubly-FED induction machine intended for a flywheel energy storage system," *IEEE Trans. Power Electron.*, vol. 17, no. 1, pp. 109–116, Jan. 2002.
[15] G. Li, J. Zhang, S. Cheng, J. Wen, and Y. Pan, "State space formulation and stability analysis of a doubly-FED induction machine with a flywheel energy storage system," in *Proc. Int. Conf. Power Syst. Technol.*, 2006, pp. 1–6.
[16] J. B. Wu, J. Y. Wen, H. S. Sun, and S. J. Cheng, "Research on dynamic operation characteristics of a doubly-FED induction machine with a flywheel energy storage system," in *Proc. Int. Conf. Sustain. Power Gener. Supply*, 2009, pp. 1–6.
[17] A. Joseph, T. R. Chelliah, R. Selvaraj, and K.-B. Lee, "Fault diagnosis and fault-tolerant control of megawatt power electronic converter-FED large-rated asynchronous hydrogenerator," *IEEE Trans. Emerg. Sel. Topics Power Electron.*, vol. 7, no. 4, pp. 2403–2416, Dec. 2019.
[18] M. Saeedifard, A. Bakhshai, and G. Joos, "Low switching frequency space vector modulators for high power multimodule converters," *IEEE Trans. Power Electron.*, vol. 20, no. 6, pp. 1310–1318, Nov. 2005.
[19] A. Luna, F. K. A. Lima, P. Rodriguez, E. H. Watanabe, and R. Teodorescu, "Comparison of power control strategies for DFIG wind turbines," in *Proc. 34th Annu. Conf. IEEE Ind. Electron.*, 2008, pp. 2131–2136.
[20] E. J. Bueno, S. Cobreces, F. J. Rodriguez, A. Hernandez, and F. Espinosa, "Design of a back-to-back NPC converter interface for wind turbines with squirrel-cage induction generator," *IEEE Trans. Energy Convers.*, vol. 23, no. 3, pp. 932–945, Sep. 2008.
[21] J.-S. Lee, E. Lee, and K.-B. Lee, "Hybrid parallel three-level converter topology for large wind turbine generation systems," in *Proc. IEEE 23rd Int. Symp. Ind. Electron.*, 2014, pp. 515–520.
[22] X. Wen, W. Kai, and Z. Shengzhe, "Research on hierarchical control strategy of hybrid energy storage system in microgrid," in *Proc. 2017 Chin. Automat. Congr.*, 2017, pp. 3323–3326.
[23] P. Wang and F. M. Niu, "Research on the AGC coordination control method including energy storage system based on area control error in the interconnected power grid," in *Proc. IEEE 2nd Int. Future Energy Electron. Conf.*, 2015, pp. 1–5.
[24] *IEEE Standard for Interconnection and Interoperability of Inverter-Based Resources (IBRS) Interconnecting With Associated Transmission Electric Power Systems*, IEEE Std 2800-2022, pp. 1–180, 2022.
[25] T. Ueda, K. Sano, D. Terazono, and K. Nada, "Instability and stabilization filter of df/dt-type virtual inertia control comparing to synchronous machines," *IEEE Open J. Power Electron.*, vol. 6, pp. 849–857, 2025.

Xianfei Xie received the B.E. and Ph.D. degrees in electrical engineering from the Huazhong University of Science and Technology, Wuhan, China, in 2011 and 2016, respectively.

He is currently with the State Key Laboratory of Advanced Electromagnetic Technology, Huazhong University of Science and Technology. His current research interests include electrical machinery and drives, pulsed power supply, and design of power electronics devices.

Patrick J. Palanas received the B.E. degree in electrical engineering in 2021 from the Huazhong University of Science and Technology, Wuhan, China, where he is currently working toward the Ph.D. degree in electrical engineering.

His current research interests include the control and design of grid-tied inverters and motor drives.

Yahong Chen received the M.E. degree in electrical engineering from the Harbin Institute of Technology, Harbin, China, in 2016 and the Ph.D. degree in electrical engineering from Wuhan University, Wuhan, in 2021.

He was a Postdoctoral Research Fellow with the State Key Laboratory of Advanced Electromagnetic Technology, Huazhong University of Science and Technology, Wuhan. He is currently with the School of Automation, Wuhan University of Technology, Wuhan.

Xiaozhe Li received the B.E. degree in electrical engineering in 2022 from Dalian Maritime University, Dalian, China, where he is currently working toward the M.E. degree in electrical engineering with the Huazhong University of Science and Technology, Wuhan, China.

His current research interests include doubly-fed motors and grid-tied inverters in the power system.

Tianqi Xie received the B.E. degree in electrical engineering in 2024 from the Huazhong University of Science and Technology, Wuhan, China, where he is currently working toward the M.E. degree in electrical engineering.

His research focuses on advanced control strategies for doubly-fed induction generators, particularly grid-forming control strategies for renewable energy integration and grid support applications.

Jiabing Hu (Senior Member, IEEE) received the B.Eng. and Ph.D. degrees in electrical engineering from the College of Electrical Engineering, Zhejiang University, Hangzhou, China, in 2004 and 2009, respectively.

From 2007 to 2008, he was funded by Chinese Scholarship Council as a visiting scholar with the Department of Electronic and Electrical Engineering, University of Strathclyde, Glasgow, U.K. From April 2010 to August 2011, he was a Postdoctoral Research Associate with Sheffield Siemens Wind Power (S2WP) Research Center and the Department of Electronic and Electrical Engineering, University of Sheffield, Sheffield, U.K. Since September 2011, he has been a Professor with the State Key Laboratory of Advanced Electromagnetic Technology, and School of Electrical and Electronic Engineering, Huazhong University of Science and Technology, Wuhan, China. His research interests include grid integration of large-scale renewables and modeling, analysis, and control of power electronized power systems.